Effect of Er^{3+} ion incorporation on the structural, photoluminescence, and ferroelectric properties of $K_{0.5}Na_{0.5}NbO_3$ ceramic for optoelectronic applications

Muskan Varshney[1] · Shreya Soni[1] · Ankita Banwal[1] · Megha Narwan[1] · Manoj Verma[2] · Renuka Bokolia[1]

Abstract

The lead-free ceramics $K_{0.5}Na_{0.5}NbO_3$: x wt% Er^{3+} (x = 0, 1, 2, 3 and 4) were produced via solid-state method. The ceramic was sintered at 1100 °C to produce a pure-phase perovskite with an orthorhombic structure. No extra phases in the XRD spectra demonstrate that all the Er^{3+} ions have dispersed into the host lattice. At room temperature, PL emission spectra were examined under the wavelengths 488 and 980 nm. In both emission spectra, green emission bands (528 and 549 nm) and slightly faint red emission bands (662 nm) were found. Observing the effect of pump power revealed that two photons are involved in the emission process. The time decay profile indicates an average lifetime of Er^{3+} ions is 25.05 μs. The ferroelectric hysteresis loop at room temperature showed decent shapes with good remnant. Thus, by combining the optical and ferroelectric properties, KNN may have potential applications to be employed in optoelectronic devices.

1 Introduction

A large amount of poisonous lead is present, and lead-based ceramics have produced major environmental and health issues. The WEEE (Waste from Electrical and Electronic Equipment) and RoHS (Restriction of Hazardous Substances) regulations have therefore prohibited the use of these ceramics [1, 2]. Researchers concentrated on lead-free ceramics such as $Na_{0.5}Bi_{0.5}TiO_3$, $BaTiO_3$, bismuth layer-structured ferroelectrics (BLSF), and various other compounds to substitute the harmful lead found in lead-based ceramics. $BaTiO_3$ (BT), $Na_{0.5}Bi_{0.5}TiO_3$ (NBT), and BLSF are some examples of lead-free ceramics. Their unique characteristics include optical transmission, ferroelectricity, dielectricity, piezoelectricity, and electro-optics, making them an exciting research topic [3]. The search for one particular lead-free alternative that is compatible with all applications in terms of its characteristics and applications has consistently been unsuccessful [4]. The previous reports on lead-free ceramics with excellent dielectric, piezoelectric, and ferroelectric properties and their comparatively low phonon energy (750 cm^{-1}) and strong physical–chemical stability were found. Among them, sodium potassium niobate (KNN) ferroelectric ceramics are the better substrates for upconversion luminescence [5–9]. From the literature survey, it has been confirmed that ferroelectric materials can display electrical and luminescence properties after being doped with rare-earth (RE^{3+}) ions [10, 11]. KNN has an ABO_3 perovskite structure [12]. It is a composition in a 1:1 ratio of ferroelectric and antiferroelectric, $KNbO_3$ and $NaNbO_3$, respectively [12, 13].

The choice of the host material is essential for achieving above-average mid-infrared (MIR) emission and vis-up-conversion efficiency for Er^{3+}. Halide glasses, particularly fluoride because of their significantly low phonon energies, have been thoroughly examined in the previous investigation as the host materials of Er^{3+}. Among RE^{3+}, finding appropriate host materials is becoming more crucial to achieve optimum up-conversion efficacy in the mid-IR and visible regions. It is discovered that the host matrix's interactions with particle dimension, RE^{3+} doping, phase purity, position replacement, and ion diffusion affect the upconversion

✉ Renuka Bokolia
renukabokolia@dtu.ac.in

1 Department of Applied Physics, CFMRL, Delhi Technological University, Delhi, India

2 Department of Physics, Hindu College, University of Delhi, Delhi, India

(UC) emission [14]. Particularly for luminescent thermometry applications, there is a need for appropriate host materials that can maintain their heat stability and responsiveness throughout a wide temperature range (around the ambient temperature) [15]. Er^{3+} is found to be the most cost-effective and abundant among all the lanthanide ions and a decent activator because of its broad photoluminescence (PL) emission range, from mid-infrared (MIR) to visible regions [4, 16, 17]. Er^{3+}-based solid-state lasers have shown promising results in laser output and can be used in the eye-safe MIR region. These lasers have many potential applications, including atmosphere pollution monitoring, medical surgery, military counter-measures, and remote sensing [10]. Due to its energy level configuration with a $^4I_{15/2}$ to $^4I_{11/2}$ transition, which is easily activated by low-energy photons, Er^{3+} is the most popular ion for upconversion [18].

In the field of optoelectronics and photovoltaics, the photo-electronic characteristics of ceramics play a vital role in determining their appropriateness. Lanthanide elements improve electrical and optical performance, enabling efficient and eco-friendly electronics [19]. Transparent ceramics like $(K_{0.5}Na_{0.5})NbO_3$-$ErBiO_3$ have good optical and ferroelectric properties, making them potential candidates for optical modulation, switchers, and electro-optical devices [20]. Sm^{3+}-doped lead-free $0.85(K_{0.5}Na_{0.5})NbO_3$-$0.15SrZrO_3$ (KNN-SZ: Sm^{3+}) transparent ferroelectric ceramics have a unique photochromic phenomenon and reversible luminescence modulation, making them ideal for information storage, displays, anti-counterfeiting, and photo-switching devices [21]. Studies also demonstrate that $(Bi_{0.5}Na_{0.5})_{0.94}Ba_{0.06}TiO_3$ lead-free ferroelectric ceramics control the dielectric constant by light exposure while maintaining superior electrical insulation. This makes these ceramics suitable for photo-dielectric devices [22].

Based on the design technique mentioned above, in this research, the structural and ferroelectric properties of Er^{3+} substituted KNN ceramics were explored to enhance radiative upconversion emission. Using Cu-Kα radiations, an X-ray diffractometer was utilized to analyze the crystalline manner and identify the KNN ceramic's phase. Further, FTIR spectroscopy was done to confirm the perovskite structure. P-E loops were investigated to study the ferroelectric properties. The optical properties, PL, and UCL emission spectra were also examined under the two excitation wavelengths, 488 nm and 980 nm, respectively.

2 Experimental procedure

2.1 Sample preparation

The solid-state reaction is a commonly used synthesis technique for creating polycrystalline materials from solid reagents. This method typically involves using very high temperatures to initiate the reaction. The chemical and morphological properties of the reagents, including their reactivity, surface area, and free energy, as well as the reaction conditions, such as temperature, pressure, and environment, can all affect the solid-state reaction. The solid-state reaction method helps produce a high volume of product is extremely easy to use compared to other techniques, and is economical [23]. The solid-state reaction was chosen in this study because it is simple, and the apparent lack of solvents makes the process economical. The solid-state reaction is preferable for commercial applications. However, to maintain stoichiometry, the starting materials, particularly K_2CO_3, must be dried due to their sensitivity to moisture [24].

The $K_{0.5}Na_{0.5}NbO_3$ (KNN) ceramics added with x wt% Er^{3+} ion abbreviated as (KNN: xEr, x = 0, 1, 2, 3, and 4). This study used a conventional solid-state reaction route to prepare the KNN ceramics. High purity (99.99%) precursors K_2CO_3, Na_2CO_3, Nb_2O_5, and Er_2O_3 from Sigma Aldrich were measured in stoichiometric ratio. Mixed powders in the stoichiometric ratio were hand-ground in a mortar pestle for 5 h using ethanol. In a small crucible made from alumina, the hand-ground powders were calcined for 3 h at varying temperatures (700–900 °C). Then, the powders with the least unreacted residue were combined with 5 wt% polyvinyl alcohol (PVA), a standard binder. After mixing, the resulting blend was compressed into a 1 mm thick pellet with a 10 mm diameter using a manual hydraulic press. The press had a pressure of 50 MPa and a resting period of 1 min. The pellets were then sintered in a furnace at 1100 °C for 2 h with intermittent heat treatment at 500 °C for 1 h to eliminate the binder from the pellets [25]. Similar steps were repeated for producing KNN: Er^{3+} ceramics. A schematic diagram is given in Fig. 1 to explain the synthesis process. Equation (1) provides the synthesis with reaction [26]:

$$K_2CO_3(s) + Na_2CO_3(s) + 2 Nb_2O_5(s)$$
$$\rightarrow 4 K_{0.5}Na_{0.5}NbO_3(s) + 2 CO_2(g) \quad (1)$$
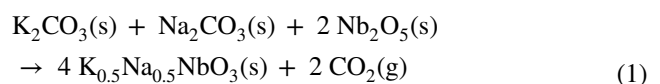
2.2 Sample characterization

X-ray diffraction (XRD) spectra were collected on a Bruker D-8 advance X-ray diffractometer with Cu-Kα radiation in the range 2θ (10°—80°), and the phase formation of synthesized samples was analyzed. The HORIBA PTI Quantamaster (8450–11) at an excitation wavelength of 980 nm was utilized to investigate the upconversion luminescence (UC) spectra. A silver paste was coated (area ~ 8.5–11 mm²) on the prepared pellets (thickness ~ 0.55–0.65 mm). The coated pellets were baked for 10 min at 500 °C so that the paste
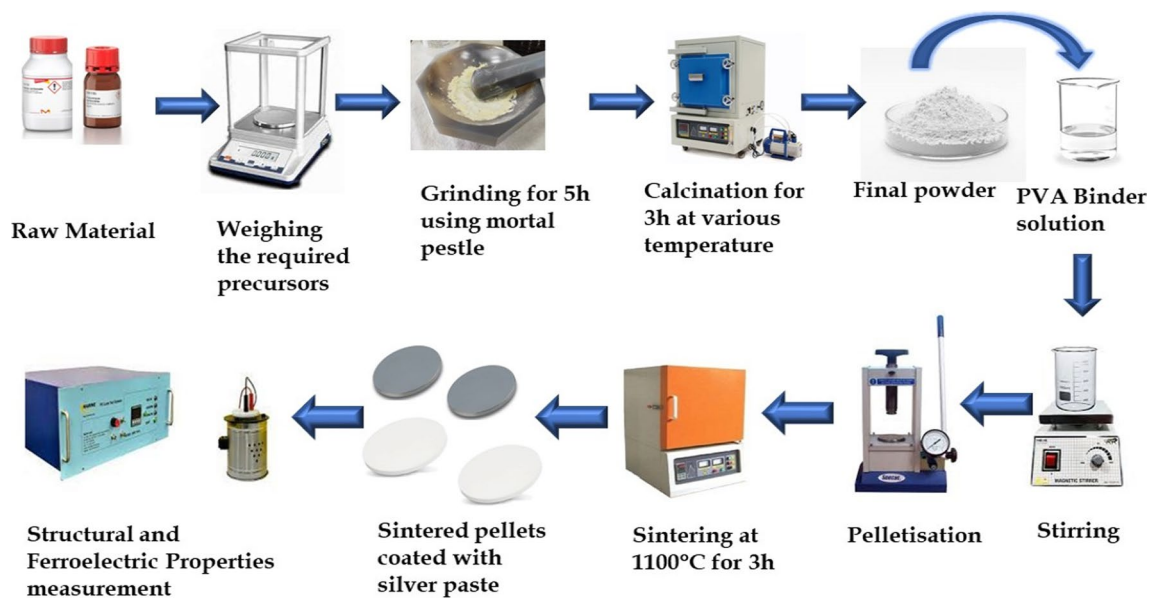
Fig. 1 A schematic illustration of the synthesis process

adhered utterly to the pellets. The P-E hysteresis loops were marked out by an automatic loop tracer under 50 Hz. SHIMADZU RF-5301 PC-spectro fluorophotometer and Xenon arc lamp were acquired to study the PL spectra under the excitation of 488 nm at room temperature. The FTIR spectra were obtained by the Perkin Elmer spectrum-II.

3 Result and discussion

3.1 XRD analysis

Figure 2a–e displays the XRD pattern of pure KNN powder calcined at various temperatures (700 °C, 750 °C, 800 °C, 850 °C, 900 °C). There are some small peaks at 15.88°, 27.76°, 30.24°, and 34.44° (depicted by symbol *), indicating that the material is not solely single-phased. Still, the slight impurities did not significantly impact the X-ray diffraction pattern. With the gradual increase in calcination temperature (700–900 °C), there is an apparent rise in X-ray reflection intensity from various planes and the intensity of secondary peaks (depicted by symbol *) reduces significantly.

At 900 °C, the unit cell structure of the crystal of the KNN sample is observed to have a strong reflection arising from the [020] plane. The peak splitting near 46° and broadening in the diffraction patterns implies that the structure is orthorhombic perovskite [27, 28]. Particularly, the (022) and (200) peaks splitting around 46°, with the (022) peak having a higher value, confirms the

orthorhombic lattice [28]. The XRD test demonstrates the existence of all anticipated Amm2 space group reflections, which matches the reference number 98–024-7571 from the inorganic crystal structure database (ICSD), which has an orthorhombic crystalline arrangement. For further investigation, 900 °C was chosen to be the optimum calcination temperature. Figure 3a depicts the XRD pattern of KNN: xEr with various concentrations of Er³⁺ sintered at 1100 °C after being calcined at 900 °C [29]. The perovskite structure is present in all the ceramics, which indicates that Er³⁺ ions have successfully diffused into the KNN host lattice. Due to the incorporation of erbium ions, the (022) and (200) peaks appear to merge indicating there may be a phase conversion [10]. The intense peak (020) moves to higher angles due to the incorporation of Er³⁺ ions, as shown in Fig. 3b. Er³⁺ ions with a smaller ionic radius of 1.23 Å occupy the A sites (K, Na) (K⁺ ionic radius = 1.64 Å, Na⁺ ionic radius = 1.39 Å) [9, 30]. This decreases the interplanar spacing (d), causing the XRD peak (002) to shift to higher angles, resulting in peak shifting. Furthermore, the decrement in interplanar spacing (d) was confirmed by calculating the a, b, and c lattice parameters of the KNN: xEr (x = 0, 1, 2, 3, 4) using the Topaz software given in Table 1. A decrease in cell volume and lattice parameters a, b, c is observed for KNN: xEr (x = 0, 1, 2, 3). Dopants possessing ionic radii that are less than those of the host material result in a reduction of the lattice parameters. This decrease is attributed to the combined influence of the small dopant and the contraction generated by the development of oxygen vacancies
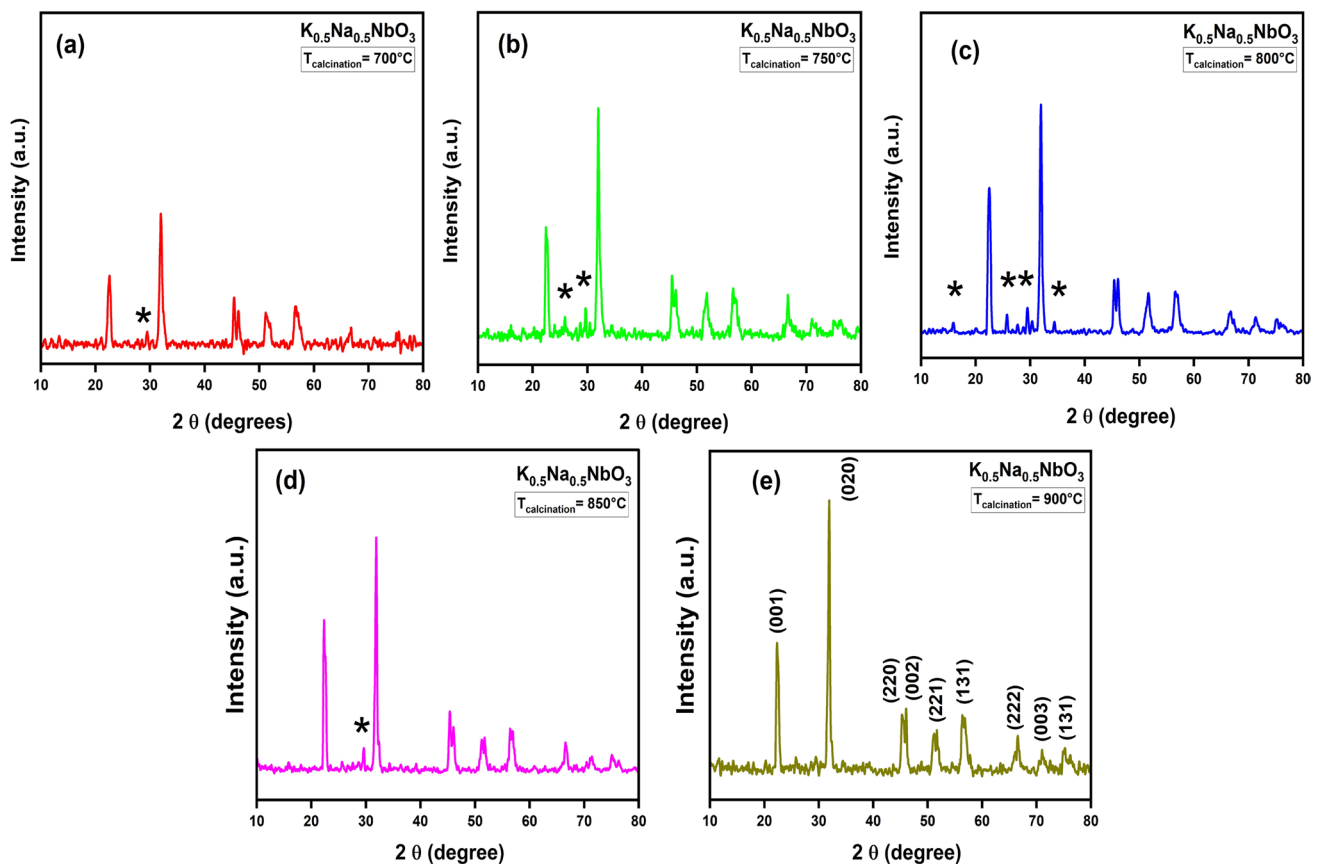
Fig. 2 a–e XRD spectra of pure KNN powders calcined at various temperatures ranging from 700 to 900 °C, as the temperature increases the intensity of impurity peaks (depicted by *) reduces significantly
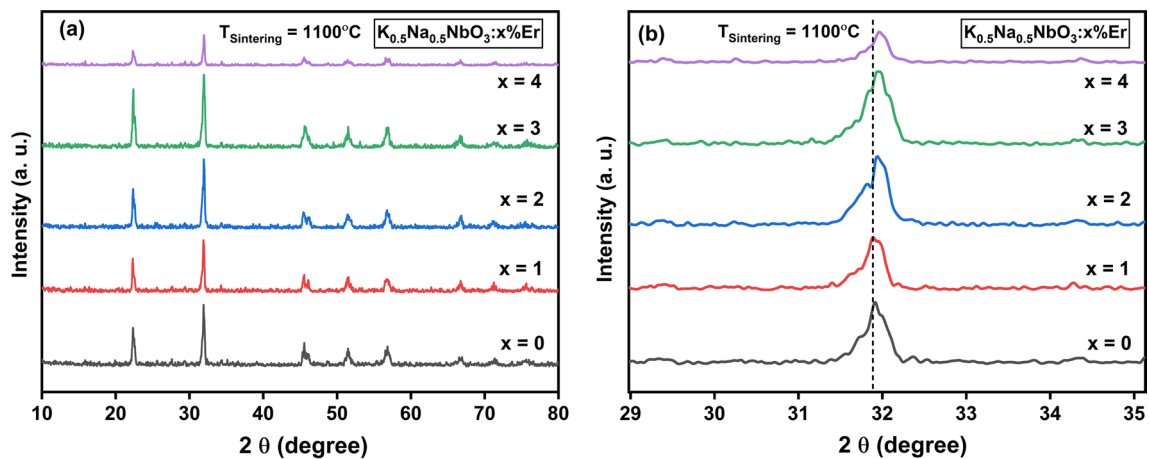
Fig. 3 a XRD spectra of KNN:xEr ceramic doped with various concentrations of Er^{3+} sintered at 1100 °C, **b** Shifting of highly intense peak to the larger 2θ angle due to incorporation of Er^{3+} ions

[31]. A slight lattice expansion is observed at x = 4, this is attributed to erbium ions not being diffused properly into the host lattice [32].

3.2 Fourier transform infrared (FTIR) spectroscopy

FTIR studies were carried out on KNN ceramics after being sintered at 1100 °C temperatures to discover more about their chemical interactions and functional groups. The FTIR

Table 1 Lattice parameters of KNN: xEr (x = 0, 1, 2, 3, 4)

Parameters	$K_{0.5}Na_{0.5}NbO_3$: x%Er^{3+}				
	x = 0.00	x = 0.01	x = 0.02	x = 0.03	x = 0.04
a(Å)	3.952386	3.939977	3.939214	3.934564	3.956896
b(Å)	5.697562	5.650172	5.660131	5.626436	5.676656
c(Å)	5.630112	5.616234	5.604401	5.604849	5.650599
Cell Volume (Å^3)	126.7843	125.0261	124.9584	124.0777	126.9234
R$_{wp}$	12.67	13.73	10.94	12.92	13.55
R$_{exp}$	9.24	9.19	9.09	8.82	9.33
R$_p$	14	15.07	12.12	14.91	15.50
GOF (χ)	1.37	1.49	1.21	1.46	1.45

spectra obtained for KNN: xEr (x = 0, 1, 2, 3, and 4) are represented in Fig. 4a. The high-intensity transmittance band at 486 cm^{-1} is accredited to the stretching and bending of the NbO$_6$ bond [13]. The less dominant band at 720 cm^{-1} is attributed to the oxygen octahedral which are the characteristic peaks of KNN [12]. In Fig. 4b, there is a peak shift from 471 cm^{-1} to 486 cm^{-1}, which leads to the conclusion that the FTIR spectra are exceptionally prone to changes in the local structure of the substance when a foreign ion is introduced [11].

3.3 Vis-down conversion photoluminescence

The excitation spectra of KNN are given in Fig. 5a and the dominant peak was observed at 488 nm via transition from ground state to $^4F_{7/2}$. Figure 5b displays the emission spectra of visible down conversion photoluminescence;
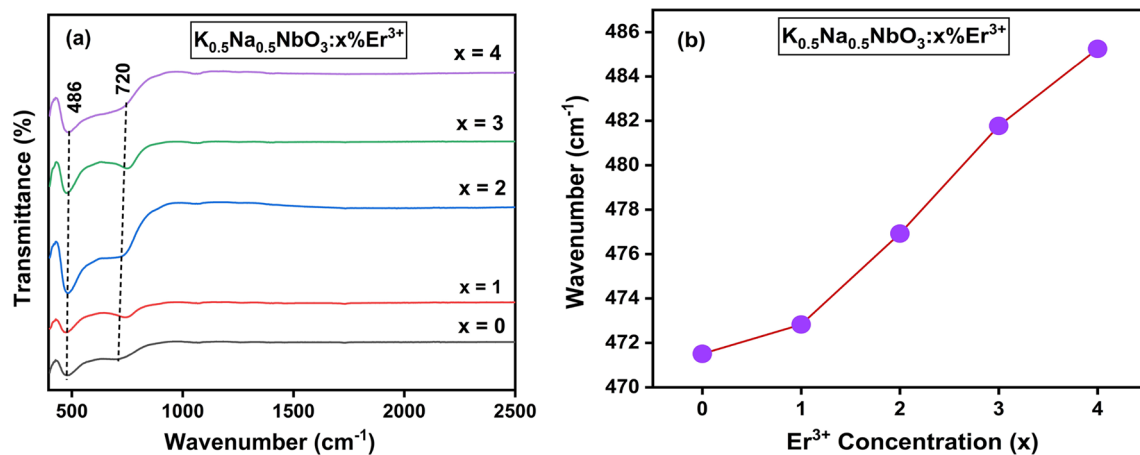
Fig. 4 a FTIR spectra of KNN: xEr ceramic, **b** Variation of FTIR mode with Er^{3+} concentrations
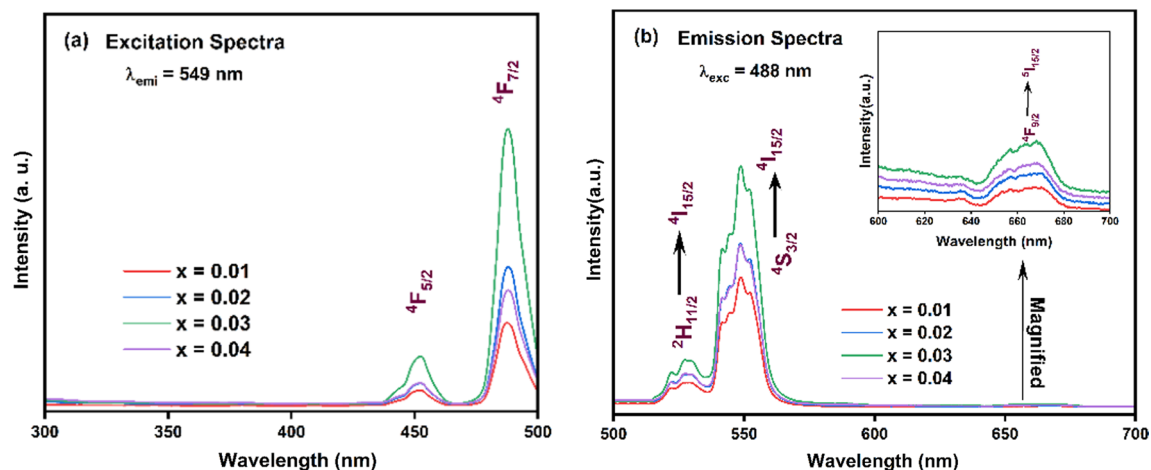
Fig. 5 a Excitation spectra of vis-down-conversion photoluminescence of KNN, **b** Emission spectra for all the KNN compositions under the excitation source of 488 nm

the $^2H_{11/2} \rightarrow {}^4S_{3/2}$ and $^2H_{11/2} \rightarrow {}^4I_{15/2}$ transitions are responsible for the dominant green radiation near 528 nm and 549 nm, correspondingly. The relatively faint red color radiation at 662 nm is attributed to the transition $^4F_{9/2} \rightarrow {}^4I_{15/2}$ [31, 33]. Under excitation by a wavelength of 488 nm, the electrons are directly excited to the $^2H_{11/2}$ and $^4S_{3/2}$ levels, which accounts for the significant intensity of both green and red color emissions via down-conversion. These levels simultaneously experience radiative and non-radiative emissions. Er^{3+} ions are stimulated to the $^4F_{7/2}$ level when the light source is 488 nm. The preponderance of stimulated Er^{3+} ions first reaches the $^4S_{3/2}$ level via non-radiative relaxation due to the highest multi-photon relaxation (MPR) rate, and then they reach the $^4I_{15/2}$ ground level via radiation relaxation. This demonstrates that Er^{3+}, and not any other particles in the KNN lattice, is the source of the green luminescence detected in the KNN [8]. The magnified view of the red band at 662 nm can be seen in the inset of Fig. 5. Therefore, the most effective illumination sources for Er-doped PL

materials should have a wavelength of 488 nm for operations involving down-conversion [34].

3.4 Vis-up conversion photoluminescence

The UC emission bands that have been detected are consistent with past studies on various hosts that have been doped with Er^{3+} [35–38]. Figure 6a displays the vis-up-conversion luminescence spectrum of KNN: xEr using a source of a diode laser lamp with a 980 nm wavelength. There are two prominent fluorescence peaks of a green color observed at 528 nm and 549 nm and a weak red band at 662 nm. The red color can be attributed to the 4f-4f transition within the Er^{3+} (inset Fig. 6a). The two primary peaks at 528 nm and 549 nm correspond with the $^2H_{11/2}$ energy level and the $^4S_{3/2}$ energy level of Er^{3+}, respectively. This causes Er^{3+} to transition to the ground state $^4I_{15/2}$ and release photons. The faint fluorescence peak of red at 662 nm corresponds to the transition from the $^4F_{9/2}$ energy level of Er^{3+} to the ground state $^4I_{15/2}$. The UCL intensity enhances with Er^{3+} concentration
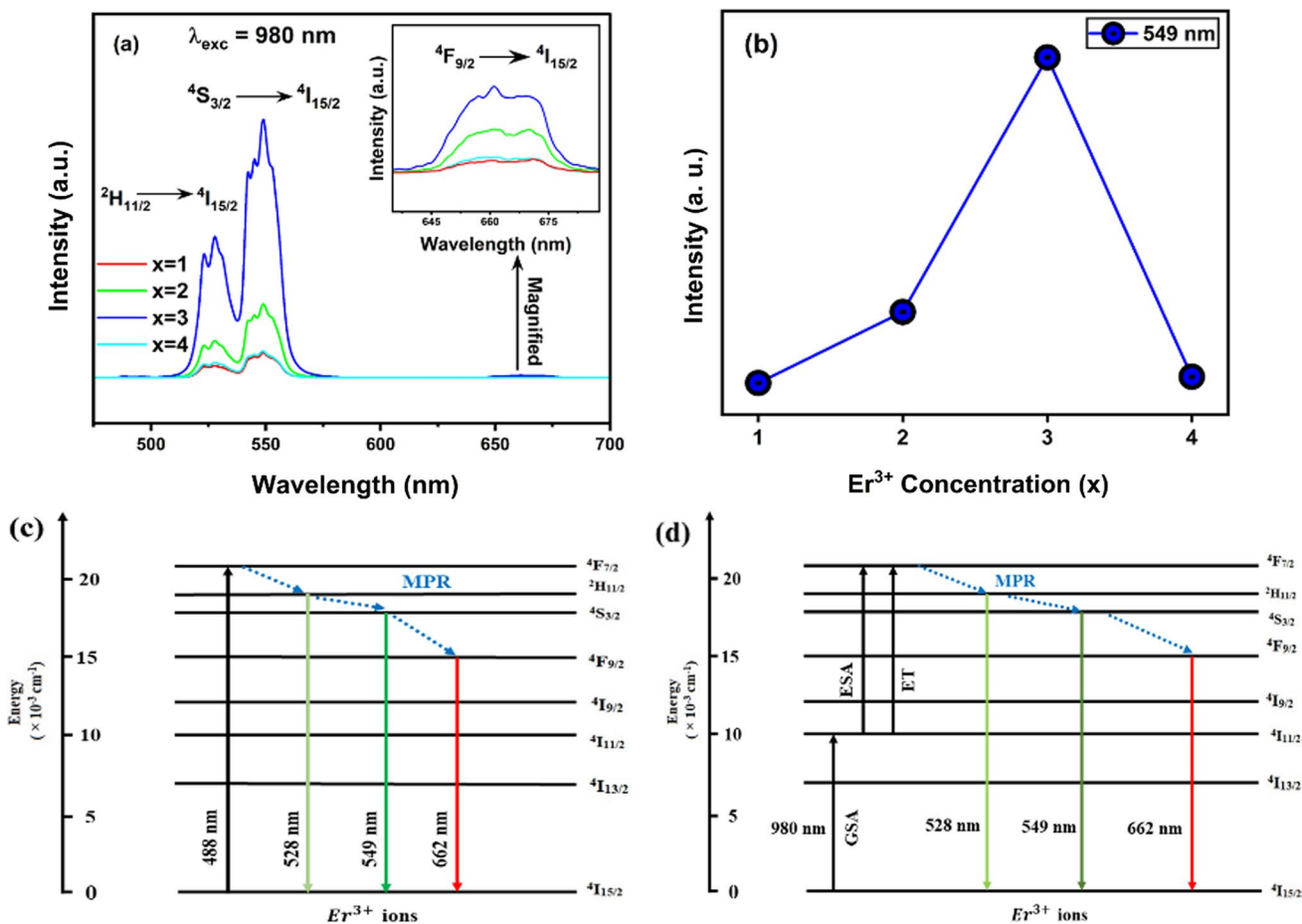
Fig. 6 **a** Vis-up-conversion emission spectra of KNN under the wavelength of 980 nm excitation, **b** Plot of intensity v/s Er^{3+} concentrations, **c** Mechanism of Er^{3+} downconversion luminescence under 488 nm light excitation (**d**) Er^{3+} upconversion luminescence mechanism when excited by 980 nm light

but subsequently reaches its maximum strength, i.e., at $x = 3$, the UCL intensity diminishes with further insertion of Er^{3+} content in the host lattice. This occurs due to the concentration-quenching effect. Figure 6b shows the variation of UCL intensity with varying Er^{3+} concentrations. The dopant concentration reaches an edge where the distance between erbium (dopant) ions becomes so minute that their energy transference becomes simpler, contributing to non-radiative relaxation. The radiative transitions reduce; hence the strength of the PL emissions diminishes [13].

Figure 6c shows the mechanism of the down-conversion process of Er^{3+} ions under the excitation of 488 nm. It has been observed that Er^{3+} ions in the ground state absorb photons and directly go to a higher energy level of $^4F_{7/2}$. However, under 488 nm excitation, the red and green emissions are low relative to the emission under 980 nm excitation. Excitation at a wavelength of 488 nm causes the electrons to be directly excited to the $^4F_{7/2}$ level. The multi-phonon

relaxation (MPR) of the $^4F_{7/2}$ energy level results in non-radiative transmission and occupies the mixed $^2H_{11/2}$ and $^4S_{3/2}$ energy levels at the same time. A restricted number of electrons reach the $^4F_{9/2}$ level simultaneously. The electrons then radiatively transition to the ground state $^4I_{15/2}$, emitting photons of the colors green and red with wavelengths of 549 and 662 nm, respectively. It demonstrates that the transitions involved in up-conversion at 980 nm differ significantly from those in excitation at 488 nm. As shown in Fig. 6d, Er^{3+} ions in the $^4I_{15/2}$ ground state are excited by the incident 980 nm photons to the $^4I_{11/2}$ level by the ground state absorption process (GSA). Some of the Er^{3+} ions in the $^4I_{11/2}$ level absorb one more incident photon to populate the $^4F_{7/2}$ level by an excited state absorption (ESA) process. Under 980 nm stimulation, numerous Er^{3+} ions are driven to the transitional level, thereby increasing the population of the $^4F_{7/2}$ energy level via energy transfer (ET), which is not possible at 488 nm [15].

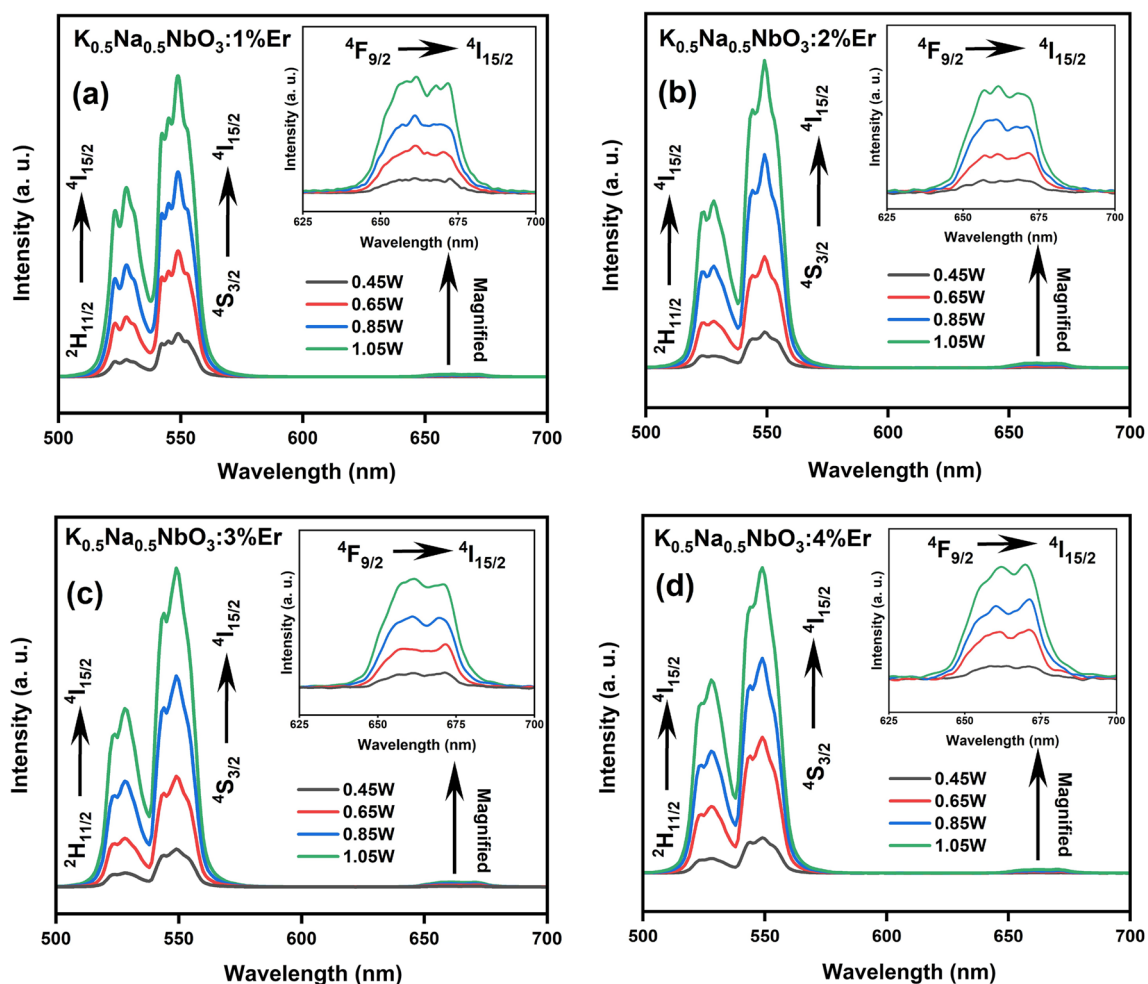**Fig. 7** **a–d** Pump power dependency on UC emission spectra with various dopant concentrations

3.5 Impact of different pump power on UCL

The total intensity of each emission band has been incorporated, and its relationship to pumping power has been plotted in Fig. 7a–d. With the rising pump power, the UCL intensity increases for all the concentrations of Er^{3+}. A power law mathematical expression among the intensity I and pump power P is suggested by theoretical analysis of the multiphoton absorption process is represented in Eq. (2) [39–41]:

$$I \propto P^n \tag{2}$$

where n signifies the amount of photons needed to complete the UCL mechanism. In the log–log plot shown in Fig. 8(a-d), three straight lines with positive slopes (denoted by n) for each dopant concentration have been calculated for all emission bands. The characteristics of the upconversion phenomenon, or the number of photons absorbed during the upconversion phenomenon, can be determined using a log–log scale to plot emission intensity versus excitation power. For the emission bands nearly at 528, 549, and 662 nm, the slope (n) is calculated by linearly fitting the experimental data and
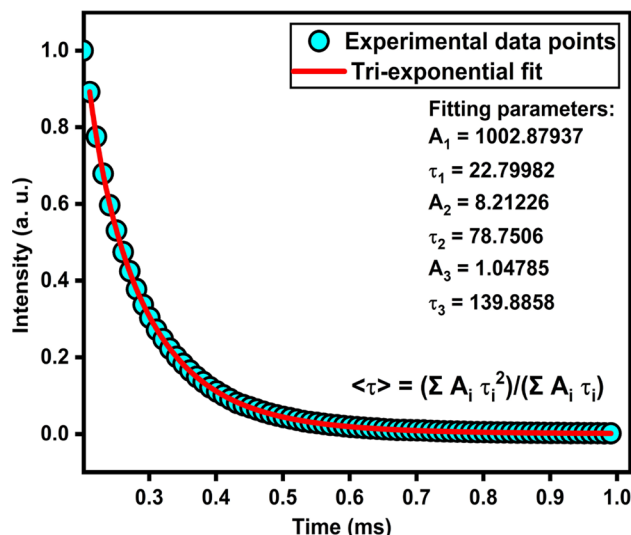
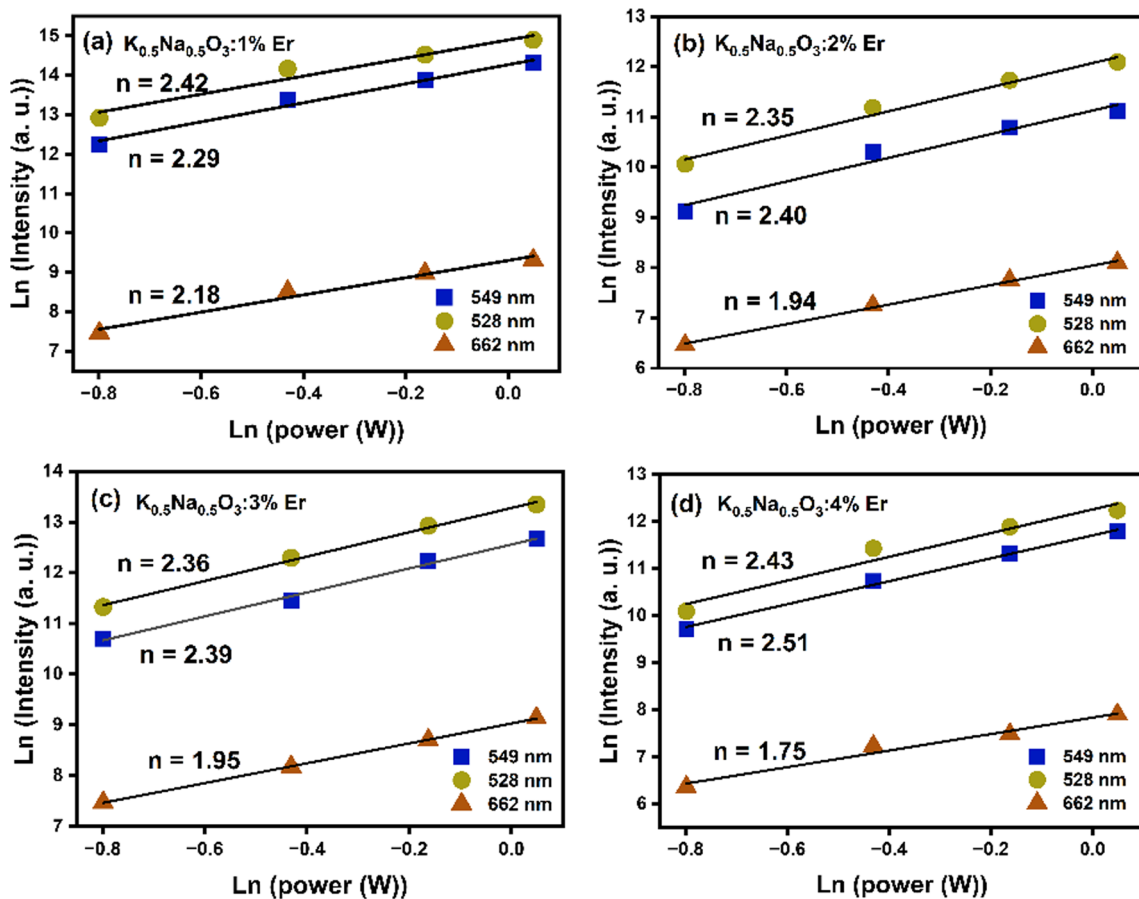**Fig. 9** Time decay profile of $K_{0.5}Na_{0.5}NbO_3$: Er^{3+}

Fig. 8 a–d Log–log plot of $K_{0.5}Na_{0.5}NbO_3$ ceramic with various Er^{3+} concentrations

it comes around 2. This shows that at least 2 pump photons are required in UC emissions [42].

3.6 Time decay analysis

The time-resolved photoluminescence (TRPL) decay curve revealed the emission at 549 nm of Er^{3+} ions when stimulated with a Xenon laser at 980 nm. Figure 9 illustrates the time decay profile associated with the $^4S_{3/2} \rightarrow ^4I_{15/2}$ level at room temperature. It was adequate to fit the decay patterns of singular doped systems with a tri-exponential decay function for Er^{3+}, as described by Eq. (3):

$$I(t) = A_0 + A_1 e_1^{-t/\tau} + A_2 e_2^{-t/\tau} + A_3 e_3^{-t/\tau} \qquad (3)$$

Here, I(t) represents the time variation of luminous intensity; A_i represents the scalar quantities; t represents the measured time; and τ_i represents the decay time when the excited state population falls to 1/e of its initial value. The generalized equation with i = 1, 2, and 3 for tri-exponential fit is used to determine the average lifespan [43]. After substituting all the values in Eq. (4), the average time was calculated to be 25.05 µs [44].

$$\tau_{avg} = \frac{\sum A_i \tau_i^2}{\sum A_i \tau_i} \qquad (4)$$

3.7 Ferroelectric properties

When describing the electrical behavior of a ferroelectric ceramic, the hysteresis loop (polarization versus electric field) is the single most crucial measurement that can be made. The name "ferroelectric" comes from the fact that this loop resembles the magnetic loop (magnetization versus magnetic field) obtained from a ferromagnetic material, even though ferroelectrics do not contain a significant amount of ferro or iron. The hysteresis loop provides information about the switching behavior of the ferroelectric material and is used to determine important parameters such as coercive field, remnant polarization, and saturation polarization. This information is essential for designing and optimizing ferroelectric devices such as capacitors, actuators, and sensors [28, 32]. Since among all doped ceramics, KNN:xEr (x = 3) showed the best upconversion intensity and XRD plot, its hysteresis loop was compared with undoped KNN. Figure 10a, b displays the P-E hysteresis loop of KNN: xEr (x = 0, 3). The hysteresis loop holds good shape for both samples, indicating KNN is a good ferroelectric. For the undoped KNN, i.e., (x = 0), the remnant polarization and coercive field increase up to 5.1 µC/cm² and 8.5 kV/cm respectively, when applied electric field increases up to 31 kV/cm. Above 31 kV/cm, the undoped KNN could not achieve the shape, resulting in lossy loops. For doped KNN: xEr (x = 3), the hysteresis loop holds its shape for the higher values of the applied electric field (31 kV/cm < E < 37 kV/cm). The remnant polarisation and coercive field decrease to 3.17 µC/cm² and 6.24 kV/cm, respectively. The observed reduction in remnant polarization is linked to the associated relaxation in the structural distortion, which can be observed from XRD and FTIR analysis. The loss of K/Na can create vacancies of oxygen, which have been observed to migrate to areas of low energy at domain walls and electrode interfaces under high electric fields. This can impede polarization switching due to domain pinning and increase coercive field [40, 45]. Table 2 elaborates on the measured values of remnant polarization and coercive field for KNN: xEr (x = 0 and 3) at various electric fields.

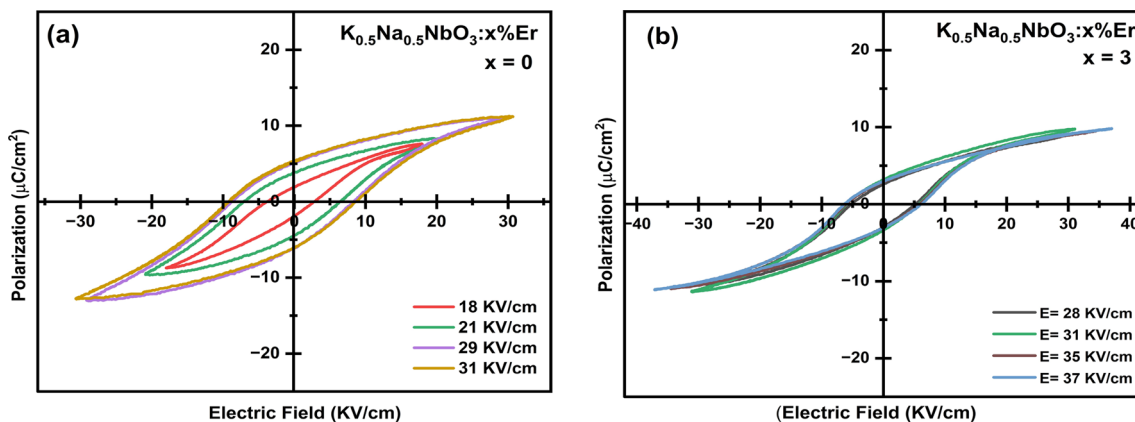**Fig. 10** **a**, **b** PE loops of KNN: xEr for x = 0 and 3 with varying electric fields

Table 2 PE parameters of KNN: xEr (x = 0 and 3) for various electric fields

Er^{3+} concentration	Electric field, E (kV/cm)	Remnant polarization, $2P_r$ ($\mu C/cm^2$)	Coercive field, $2E_c$ (kV/cm)
x = 0	18	3.702	5.462
	21	7.592	13.474
	29	10.202	17.124
x = 3	28	5.192	10.384
	31	6.356	11.364
	35	5.788	11.798
	37	6.058	12.478

4 Conclusion

The lead-free ceramic potassium sodium niobate ($K_{0.5}Na_{0.5}NbO_3$) mixed with the rare earth element Er^{3+} abbreviated KNN: xEr (where x = 0, 1, 2, 3, and 4) is made by solid-state method to investigate the effect that Er^{3+} have on structural, ferroelectric, and photoluminescence characteristics. To generate a distinct phase perovskite crystal with an orthorhombic crystal structure, the undoped KNN was first calcined at temperatures gradually increasing from 700 to 900 °C and then sintered at a temperature of 1100 °C for 3 h. Because no other phases are present in the XRD spectra of the Er^{3+}-enriched KNN, it can be deduced that all of the Er^{3+} ions have been incorporated into the host lattice. The development of a perovskite structure could be seen in the FTIR spectrum observed near 486 cm^{-1} and 720 cm^{-1}. The PL emission spectra of Er^{3+} concentrated KNN particles were analyzed at room temperature to an illumination wavelength of 488 nm and 980 nm. Both emission spectra contained bands of green emission that were quite intense (528 nm and 549 nm) and bands of red emission that were slightly less intense (662 nm). At an illumination wavelength of 980 nm, it was discovered that the upconversion PL spectra exhibited a significantly greater emission intensity than the vis-down conversion PL. It was determined that ceramics use a two-photon pumping process for the emission process after observing the influence of pump strength on the emission process. The ferroelectric PE loop was observed to have good loop shapes at room temperature and satisfactory remnant polarization for the doped and undoped KNN ceramic. This type of material possesses outstanding intrinsic piezoelectric capabilities, and by combining its optical and ferroelectric properties, it may also have the potential to be utilized as a multifunctional optoelectronic device.

References

1. R. Groß, D. Bunke, C.-O. Gensch, S. Zangl, and A. Manhart, Study on Hazardous Substances in Electrical and Electronic Equipment, Not Regulated by the RoHS Directive Final Report Content, 2008
2. X. Vendrell, J.E. García, X. Bril, D.A. Ochoa, L. Mestres, G. Dezanneau, Improving the functional properties of ($K_{0.5}Na_{0.5}$)NbO_3 piezoceramics by acceptor doping. J. Eur. Ceram. Soc. **35**(1), 125–130 (2015). https://doi.org/10.1016/j.jeurceramsoc.2014.08.033
3. H. Wu, S. Shi, X. Liu, H. Wang, J. Xu, L. Yang, W. Qiu, S. Zhou, Photoluminescence and outstanding transparent in Er^{3+}-doped ($K_{0.5}Na_{0.5}$)NbO_3-($Sr_{0.5}Ba_{0.5}$)($Bi_{0.5}Nb_{0.5}$)O_3 ceramics. J. Mater. Sci. Mater. Electron. **34**, 612 (2023). https://doi.org/10.1007/s10854-023-10021-9
4. J.P. Sharma, D. Kumar, A.K. Sharma, Structural and dielectric properties of pure potassium sodium niobate (KNN) lead-free ceramics. Solid State Commun. (2021). https://doi.org/10.1016/j.ssc.2021.114345
5. Q. Zhang, L. Luo, J. Gong, P. Du, W. Li, G. Yuan, Photoluminescence, thermoluminescence and reversible photoluminescence modulation of multifunctional optical materials Pr^{3+} doped $K_xNa_{1-x}NbO_3$ ferroelectric ceramics. J. Eur. Ceram. Soc. **40**(12), 3946–3955 (2020). https://doi.org/10.1016/j.jeurceramsoc.2020.05.003
6. Y.Y.S. Cheng, L. Liu, Y. Huang, L. Shu, Y.X. Liu, L. Wei, J.F. Li, All-inorganic flexible (K, Na)NbO_3-based lead-free piezoelectric thin films spin-coated on metallic foils. ACS Appl. Mater. Interfaces **13**(33), 39633–39640 (2021). https://doi.org/10.1021/acsami.1c11418
7. M. Dolhen, A. Mahajan, R. Pinho, M.E. Costa, G. Trolliard, P.M. Vilarinho, Sodium potassium niobate ($K_{0.5}Na_{0.5}NbO_3$, KNN) thick films by electrophoretic deposition. RSC Adv. **5**(6), 4698–4706 (2015). https://doi.org/10.1039/c4ra11058g
8. W. Li, D. Wang, X. Li, P. Li, P. Fu, C. Hu, J. Hao, W. Li, Q. Zhang, Optical temperature sensing properties and thermoluminescence behavior in Er-modified potassium sodium niobate-based multifunctional ferroelectric ceramics. J. Mater. Chem. C Mater. **10**(33), 11891–11902 (2022). https://doi.org/10.1039/d2tc01268e

9. L. Xiang, H. Gangbin, W. Huangtao, S. Shaoyang, W. Hua, X. Jiwen, Y. Ling, Q. Wei, Transmittance, photoluminescence and electrical properties in Er-doped $0.98K_{0.5}Na_{0.5}NbO_3$-$0.02Sr(Yb_{0.5}Ta_{0.5})O_3$ ferroelectric ceramics. J. Electron. Mater. **51**(7), 3476–3484 (2022). https://doi.org/10.1007/s11664-022-09626-3

10. X. Wu, S. Lu, K.W. Kwok, Photoluminescence, electro-optic response and piezoelectric properties in pressureless-sintered Er-doped KNN-based transparent ceramics. J. Alloys Compd. **695**, 3573–3578 (2017). https://doi.org/10.1016/j.jallcom.2016.11.409

11. A. Banwal, R. Bokolia, Efficient tunable temperature sensitivity in thermally coupled levels of Er^{3+}/Yb^{3+} co-doped $BaBi_2Nb_2O_9$ ferroelectric ceramic. J. Lumin. **263**, 120071 (2023). https://doi.org/10.1016/j.jlumin.2023.120071

12. S. Kumar, N. Thakur, Effect of alkali metal (Na, K) ion ratio on structural, optical and photoluminescence properties of $K_{0.5}Na_{0.5}NbO_3$ ceramics prepared by sol-gel technique. Bull. Mater. Sci. (2021). https://doi.org/10.1007/s12034-020-02341-x

13. S. Bairagi, S.W. Ali, Effects of surface modification on electrical properties of KNN nanorod-incorporated PVDF composites. J. Mater. Sci. **54**, 11462–11484 (2014). https://doi.org/10.1007/s10853-019-03719-x

14. Y. Zhang, L. Duan, A. Zhang, D. Wang, R. Chu, Z. Xu, G. Li, C. Zhang, Photoluminescence, electrical properties and electron band structure of $(Ho, Yb)^{3+}$ co-doped $SrBi_4Ti_4O_{15}$ multifunctional ceramics. Ceram. Int. **48**(7), 9248–9257 (2022). https://doi.org/10.1016/j.ceramint.2021.12.111

15. R. Bokolia, O.P. Thakur, V.K. Rai, S.K. Sharma, K. Sreenivas, Dielectric, ferroelectric and photoluminescence properties of Er^{3+} doped $Bi4Ti_3O_{12}$ ferroelectric ceramics. Ceram. Int. **41**(4), 6055–6066 (2015). https://doi.org/10.1016/j.ceramint.2015.01.062

16. X. Wu, C.M. Lau, K.W. Kwok, Effect of phase transition on photoluminescence of Er-doped KNN ceramics. J. Lumin. **155**, 343–350 (2014). https://doi.org/10.1016/j.jlumin.2014.07.005

17. M. Narwan, A. Banwal, R. Sharma, R. Bokolia, Non-invasive thermal sensing and improved recoverable energy storage density of Bi0.5Na0.5TiO3: Er3+ doped multifunctional ferroelectric ceramic. J. Lumin. **265**, 120236 (2024). https://doi.org/10.1016/j.jlumin.2023.120236

18. J. Wangi, Y. Sun, S. Shi, H. Wang, J. Xu, L. Yang, W. Qi, Effects of Er3+ doping on the structure and electro-optical properties of $0.94(K_{0.5}Na_{0.5})NbO_3$–$0.06Sr(Zn1/3Nb2/3)O_3$ ceramics. Bull. Mater. Sci. (2022). https://doi.org/10.1007/s12034-021-02596-y

19. L.N. Liu, X.M. Chen, R.Y. Jing, H.L. Lian, W.W. Wu, Y.P. Mou, P. Liu, Electrical and photoluminescence properties of $(Bi_{0.5-x/0.94}Er_{x/0.94}Na_{0.5})_{0.94}Ba_{0.06}TiO_3$ lead-free ceramics. J. Mater. Sci. Mater. Electron. **30**, 5233–5239 (2019). https://doi.org/10.1007/s10854-019-00822-2

20. C. Lin, X. Wu, M. Lin, Y. Huang, J. Li, Optical, luminescent and optical temperature sensing properties of $(K_{0.5}Na_{0.5})NbO_3$-ErBiO3 transparent ceramics. J. Alloy. Compd. **706**, 156–163 (2017). https://doi.org/10.1016/j.jallcom.2017.02.245

21. Y.J. Du, L.I.D.J. Martin, D. Poelman, Reversible yellow-gray photochromism in potassium-sodium niobate-based transparent ceramics. J. Eur. Ceram. Soc. **41**, 1925–1933 (2021). https://doi.org/10.1016/j.jeurceramsoc.2020.10.046

22. L.N. Liu, X.M. Chen, Y.D. Xu, H.L. Lian, P. Liu, Light-triggered "on-off" switchable dielectric constant in $(Bi_{0.5}Na_{0.5})_{0.94}Ba_{0.06}TiO_3$ lead-free ceramics. Appl. Phys. Lett. **123**, 022904 (2023). https://doi.org/10.1063/5.0153351

23. M.S. El-Eskandarany, Mechanically induced solid-state reduction. Mech. Alloy. (2015). https://doi.org/10.1016/B978-1-4557-7752-5.00006-1

24. L. Kozielski, K. Feliksik, B. Wodecka-Duś, D. Szalbot, S. Tutu, Hot pressed $K_{0.5}Na_{0.5}NbO_3$ material for piezoelectric transformer for energy harvesting. Arch. Metall. Mater. **63**(3), 1275–1280 (2018). https://doi.org/10.24425/123801

25. A. Banwal, R. Bokolia, Phase evolution and microstructure of $BaBi_2Nb_2O_9$ ferroelectric ceramics. Mater. Today Proc. **46**, 10121–10124 (2021). https://doi.org/10.1016/j.matpr.2020.09.380

26. H.C. Thong, C. Zhao, Z. Zhou, C.F. Wu, Y.X. Liu, Z.Z. Du, J.F. Li, W. Gong, K. Wang, Technology transfer of lead-free (K, Na) NbO_3-based piezoelectric ceramics. Mater. Today **29**, 37–48 (2019). https://doi.org/10.1016/j.mattod.2019.04.016

27. A. Dahiya, O. P. Thakur, and J. K. Juneja, Sensing and actuating applications of potassium sodium niobate: Use of potassium sodium niobate in sensor and actuator, in Proc. of the Int. Conf. on Sens. Tech. ICST, pp. 383–386, (2013), doi: https://doi.org/10.1109/ICSensT.2013.6727680

28. Q. Jin, M. Jiang, S. Han, Y. Yan, Microstructure, optical and electrical properties of Bi and Ba co-doped $K_{0.52}Na_{0.48}NbO_3$ transparent ceramics. J. Mater. Sci. Mater. Electron. **29**(15), 13407–13417 (2018). https://doi.org/10.1007/s10854-018-9466-5

29. S. Dwivedi, T. Pareek, S. Kumar, Structure, dielectric, and piezoelectric properties of $K_{0.5}Na_{0.5}NbO_3$-based lead-free ceramics. RSC Adv. **8**(43), 24286–24296 (2018). https://doi.org/10.1039/c8ra04038a

30. L. Gao, Z. Liu, P. Ren, R. Liang, T. Li, K. Guo, B. Xie, J. Lu, P. Mao, J. Tian, L. Shu, Inhibiting oxygen vacancies and twisting NbO_6 octahedron in erbium modified KNN-based multifunctional ceramics. J. Materiomics (2023). https://doi.org/10.1016/j.jmat.2023.05.007

31. E. Makagon, O. Kraynis, R. Merkle, J. Maier, I. Lubomirsky, Non-classical electrostriction in hydrated acceptor doped $BaZrO_3$: proton trapping and dopant size effect. Adv. Funct. Mater. **31**, 2104188 (2021). https://doi.org/10.1002/adfm.202104188

32. H. Sun, Q. Zhang, X. Wang, M. Gu, Green and red upconversion luminescence of Er^{3+}-doped $K_{0.5}Na_{0.5}NbO_3$ ceramics. Ceram. Int. **40**(2), 2581–2584 (2014). https://doi.org/10.1016/j.ceramint.2013.10.089

33. A. Banwal, R. Bokolia, Enhanced upconversion luminescence and optical temperature sensing performance in Er^{3+} doped $BaBi_2Nb_2O_9$ ferroelectric ceramic. Ceram. Int. **48**(2), 2230–2240 (2022). https://doi.org/10.1016/J.CERAMINT.2021.09.314

34. W.U. Xiao, *Rare-earth-doped KNN-based ceramics for photoluminescent and electro-optic applications* (The Hong Kong Polytechnic College, Hong Kong, 2015)

35. D. Peng, H. Zou, Upconversion luminescence, ferroelectrics and piezoelectrics of Er doped $SrBi_4Ti_4O_{15}$. AIP Adv. (2012). https://doi.org/10.1063/1.4773318

36. W. Li, Z. Xu, R. Chu, P. Fu, G. Zang, Improved piezoelectric property and bright upconversion luminescence in Er doped $(Ba_{0.99}Ca_{0.01})(Ti_{0.98}Zr_{0.02})O_3$ ceramics. J. Alloys Compd. **583**, 305–308 (2014). https://doi.org/10.1016/j.jallcom.2013.08.103

37. H. Liu, J. Wang, H. Wang, J. Xu, C. Zhou, W. Qiu, Er^{3+} and $Sr(Bi_{0.5}Nb_{0.5})O_3$-modified $(K_{0.5}Na_{0.5})NbO_3$: a new transparent fluorescent ferroelectric ceramic with high light transmittance and good luminescence performance. Ceram. Int. **48**(3), 4230–4237 (2022). https://doi.org/10.1016/j.ceramint.2021.10.215

38. Z. Cao, J. Wang, C. Zhang, X. Mao, L. Luo, Flexible piezoelectric nanogenerator based on the Er3+ doped lead-free $(Na_{0.5}Bi_{0.5})$ TiO3-BaTiO3 piezoelectric nanofibers with strong upconversion luminescence. J. Alloys Compd. (2022). https://doi.org/10.1016/j.jallcom.2022.165766

39. M.K. Mahata, T. Koppea, T. Mondal, C. Brüsewitza, K. Kumar, V.K. Rai, H. Hofsässa, U. Vetter, Incorporation of Zn^{2+} ions into $BaTiO_3$:Er^{3+}/Yb^{3+} nanophosphor: an effective way to enhance upconversion, defect luminescence and temperature sensing. PCCP **17**(32), 20741–20753 (2015). https://doi.org/10.1039/c5cp01874a

40. D.B. Paulaviciene, N. Traskina, R. Vargalis, A. Katelnikovas, S. Sakirzanovas, Thermal decomposition synthesis of Er^{3+}-activated $NaYbF_4$ upconverting microparticles for optical temperature sensing. J. Lumin. (2019). https://doi.org/10.1016/j.jlumin.2019.116672

41. R. Bokolia, O.P. Thakur, V.K. Rai, S.K. Sharma, K. Sreenivas, Electrical properties and light up conversion effects in $Bi_{3.79}Er_{0.03}Yb_{0.18}Ti_{3-x}W_xO_{12}$ ferroelectric ceramics. Ceram. Int. **42**(5), 5718–5730 (2016). https://doi.org/10.1016/j.ceramint.2015.12.103

42. A. Banwal, R. Bokolia, Thermometric sensing performance in Erbium modified $SrBi_{2-x}Nb_2Er_xO_9$ ferroelectric ceramic for optoelectronic devices. Ceram. Int. **48**(23), 34405–34414 (2022). https://doi.org/10.1016/j.ceramint.2022.08.019

43. Q. Zhang, K. Chen, L. Wang, H. Sun, X. Wang, X. Hao, A highly efficient, orange light-emitting $(K_{0.5}Na_{0.5})NbO_3$:Sm^{3+}/Zr^{4+} lead-free piezoelectric material with superior water resistance behavior.

J. Mater. Chem. C. Mater. **3**(20), 5275–5284 (2015). https://doi.org/10.1039/c4tc02995j

44. L. Wang, B. Lua, X. Liu, Y. Shi, J. Li, Y. Liu, Fabrication and upconversion luminescence of novel transparent Er_2O_3 ceramics. J. Eur. Ceram. Soc. (2019). https://doi.org/10.1016/j.jeurceramsoc.2019.11.048

45. Y.A. Genenko, J. Glaum, M.J. Hoffmann, K. Albe, Mechanisms of aging and fatigue in ferroelectrics. MSEB **192**(C), 52–82 (2015). https://doi.org/10.1016/j.mseb.2014.10.003